IL NUOVO CIMENTO **48 C** (2025) 6
DOI 10.1393/ncc/i2025-25006-5

Colloquia: WPCF-Resonance 2023

Heavy flavour hadronization from AA to pp collisions

S. Plumari([1])([2])([*]), V. Minissale([1])([2]) and V. Greco([1])([2])

([1]) *Department of Physics and Astronomy "E. Majorana", University of Catania Via S. Sofia 64, I-95123 Catania, Italy*
([2]) *Laboratori Nazionali del Sud, INFN-LNS - Via S. Sofia 62, I-95123 Catania, Italy*

received 23 July 2024

Summary. — One of the current challenges in understanding heavy-quark hadronization lies in interpreting measurements of heavy baryon production across various collision systems like AA, pA, and pp collisions. Predictions based on coalescence and fragmentation hadronization approaches have shown a baryon/meson ratio Λ_c/D^0 on the order of unity in AA collisions. This was initially observed at RHIC energies and more recently in pp, pA, and AA collisions at the LHC energies. The ratio in smaller collision systems suggests a significant departure from that observed in elementary collision systems, where the Λ_c/D^0 ratio is typically on the order of 10^{-1}. We present an hadronization mechanism based on the coalescence and fragmentation processes. We show that within this model it is possible describe several observables involving heavy-flavour hadrons from AA collision to pp collisions. The results suggest that a description of charmed hadron production in smaller systems like in pp collisions require the assumption of an hot QCD medium. Furthermore, we will explore particle yields of multi-charmed baryons like Ξ_{cc}, Ω_{cc} and Ω_{ccc}. Finally, we discuss the charmed and multi-charmed hadrons production in PbPb collisions within the $0-10\%$ centrality class and furthermore we show the predictions of multi-charmed hadrons in different collision systems like $Pb+Pb$, $Kr+Kr$, $Ar+Ar$ and $O+O$.

1. – Introduction

The primary objective of the heavy-ion collisions programs, such as the Large Hadron Collider (LHC) and the Relativistic Heavy-Ion Collider (RHIC), is to characterize Quark-Gluon Plasma (QGP), a state of matter believed to form during these collisions. Studies in this field have indicated the existence of a new state of matter composed of deconfined quarks and gluons, which exhibit a behavior close to that of a perfect fluid with a low shear viscosity to entropy density ratio of $4\pi\eta/s \approx 1-2$.

([*]) E-mail: salvatore.plumari@dfa.unict.it

Investigations into the production of heavy quark hadrons have been regarded as among the most effective tools to characterize the QGP [1-3]. Charm and bottom quarks are utilized as probes useful to get information about the entire evolution of QGP. Given their significant large masses, their production can be described by perturbative Quantum Chromodynamics (pQCD) calculations, and their formation time is expected to be shorter than the lifetime of the fireball produced, with $\tau_0 < 0.08 fm/c \ll \tau_{QGP}$. On the other hands, the thermalization time is expected to be much longer compared to the lifetime of the fireball, enabling heavy quarks (HQs) to trace the complete evolution of the plasma and retain information about the system's history until the final hadrons are formed.

Over the past decades, numerous studies have explored the effects of interactions between heavy quarks and bulk particles [4-16]. However, the study of Heavy Flavor production not only provides insights into heavy-flavor transport coefficients within the QGP but also sheds light on the mechanisms of heavy flavor hadronization. In both heavy-ion and proton-proton collisions, experimental data on charmed hadrons revealed an enhancement in the charmed baryon/meson ratio comparable to that observed for light and strange hadrons, which differs from ratios observed in elementary collisions such as e^+e^- and $e^{\pm}p$ [17]. These findings currently pose a challenge to the theoretical comprehension of heavy-quark hadronization. Indeed, at energies of $\sqrt{s} = 5$ TeV and 13 TeV at the LHC, in the low p_T region, the $\Lambda_c/D^0 \approx 0.5$. Moreover, the ALICE collaboration has measured the ratio of other charmed baryons such as Ξ_c and Ω_c with the D^0, revealing unexpected behavior in pp collisions [18]. These experimental findings in smaller collision systems suggest a strong correlation between heavy flavor production and the formation of Hot QCD matter [19-21].

In recent years, several groups have developed transport approaches to describe the dynamics of heavy quarks created in heavy-ion collisions to their detection as heavy hadrons in experiments. Despite successfully describing experimental data, different implementations lead to significant uncertainties in the extraction of transport coefficients and in scientific conclusions. Recent comparative studies have identified similarities and differences between models, enhancing understanding of heavy quark dynamics in the QGP. The coalescence model stands as one of the viable microscopic frameworks to explain the process of hadronization within the Quark-Gluon Plasma (QGP). This model has provided a successfully way to explain the p_T spectra of baryons and mesons, along with the splitting of elliptic flow observed between light mesons and baryons in heavy-ion collisions at top RHIC and LHC energies [22,23]. Moreover, it has predicted a significant $\Lambda_c/D^0 \sim 0.5 - 1$ ratio in AA collisions [24, 25]. Other model based on recombination on 4-momentum conservation and considering space-momentum correlations between heavy quarks and a hydrodynamically expanding bulk have shown an enhancement of the heavy flavour production, especially near the QGP fireball's surface [26]. In these models are included baryon states that are not present in Particle Data Group but are supported by Quark model predictions which permit the model to be able to describe the Λ_c/D^0 ratio also in pp collisions [27]. Other coalescence models like in [7] the heavy quark evolution is modeled via a Langevin equation, including quasi-elastic scattering and gluon radiation induced by the medium. Bulk properties are derived from hydrodynamic simulations, and hadronization involves recombination and fragmentation followed by an ultra-relativistic quantum molecular dynamics cascade. This model have shown the relevance of both radiative and collisional energy loss and hybrid hadronization approach and hadronic rescattering to get a good description of R_{AA} and v_2. Finally, Statistical Hadronization Models have been extended in [28] to incorporate heavy hadrons, assuming thermalized charm quarks and employing blast-wave modeling for transverse momentum distributions and resonance decay. or a recent systematical comparison between different hadronization models one can see ref. [29]. However, recent studies have extended this analysis to bottom hadrons in pp collisions [30] and to multi-charmed hadrons [28, 31] in different collisions systems.

2. – Hadronization by coalescence and fragmentation

In this section, we discuss the foundational aspects of the coalescence model. The momentum spectrum of hadrons resulting from quark coalescence is expressed by the equation:

$$\frac{dN_H}{dyd^2P_T} = g_H \int \prod_{i=1}^{N_q} \frac{d^3p_i}{(2\pi)^3E_i} p_i \cdot d\sigma_i \; f_{q_i}(x_i, p_i) f_H(x_1..., p_1...) \, \delta^{(2)} \left(P_T - \sum_{i=1}^{n} p_{T,i} \right) \tag{1}$$

g_H represents the statistical factor related to the formation of a colorless hadron from quarks and antiquarks. The symbol $d\sigma_i$ denotes an element of a space-like hypersurface, while f_{q_i} stands for the phase-space distribution functions of the i-th quark (anti-quark). The Wigner function $f_H(x_1...x_{N_q}, p_1...p_{N_q})$ characterizes the spatial and momentum distributions of quarks within a hadron. In the above equation when $N_q = 2$ it describes meson formation, whereas for $N_q = 3$, it describes baryon formation. The Wigner function adopted assumes a Gaussian shape in both space and momentum, expressed as $f_H(...) = \prod_{i=1}^{N_q-1} A_W \exp\left(- \frac{x_{ri}^2}{\sigma_{ri}^2} - p_{ri}^2 \sigma_{ri}^2 \right)$, where x_{ri} and p_{ri} denote the 4-vectors for relative coordinates, and A_W is a normalization constant ensuring that all charm hadrons coalesce in the limit as momentum approaches zero. The widths σ_{ri} of $f_H(...)$ are related to the size of the hadron, particularly to the root mean square charge radius of the meson; further details can be found in refs. [19, 25]. As shown in previous studies on coalescence [7, 23-25, 32], the coalescence probability decreases with increasing p_T. This trend leads to independent fragmentation becoming the dominant contribution of hadron production for high-p_T. In our approach, we include a smooth transition from low to high p_T regimes by introducing a fragmentation probability $P_{frag}(p_T)$. A charm quark with $p_T \neq 0$ undergoes hadronization through either coalescence or fragmentation. Given the hadronization probability $P_{coal}(p_T)$ for coalescence, a complementary probability for fragmentation is introduce as $P_{frag}(p_T) = 1 - P_{coal}(p_T)$. Consequently, the momentum spectra of hadrons resulting from charm parton fragmentation is expressed as

$$\frac{dN_{had}}{d^2p_T, dy} = \sum \int dz \frac{dN_{fragm}}{d^2p_T, dy} \frac{D_{had/c}(z, Q^2)}{z^2} \tag{2}$$

where $D_{had/c}(z, Q^2)$ represents the fragmentation function and $z = p_{had}/p_c$ denotes the momentum fraction transferred from heavy quarks to the final heavy hadron. In the results shown, the Peterson fragmentation function is employed [33].

3. – Charmed hadrons from AA to pp collisions

In the left panel of fig. 1, the different contributions to D meson and Λ_c baryon production from Coalescence and fragmentation have been shown. It is shown that at RHIC energies, the contributions of coalescence and fragmentation to D meson production are

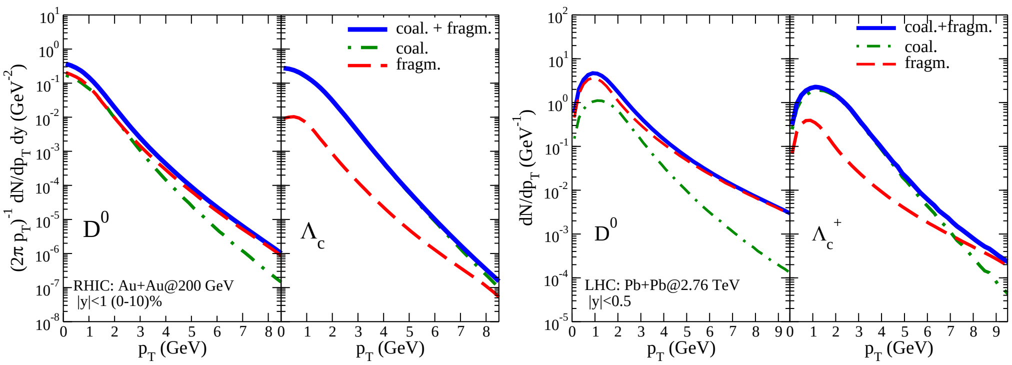

Fig. 1. – Left: Transverse momentum spectra for D^0, and Λ_c baryon at mid-rapidity for AuAu collisions at RHIC energies. Green dot-dashed and red dashed lines refer to the spectra from only coalescence and only fragmentation respectively, the blue solid line is the sum of fragmentation and coalescence. Right: Transverse momentum spectra for D^0, and Λ_c baryon at mid-rapidity for PbPb collision at LHC energies. Same legend as in left panel.

similar for $p_T < 3-4, GeV$ and fragmentation becomes dominant at higher transverse momentum. At higher collision energies such as those at LHC, a different behavior is expected, particularly the fragmentation is expected to give a larger contribution to D meson production and in the high p_T region, fragmentation emerges as the dominant mechanism at both energies. On the other hand, the contribution of baryon production id dominated by coalescence at low and in the intermediate transverse momentum region as shown by red dashed lines in fig. 1. This different contributions of coalescence mechanism are responsible for a Baryon enhancement with the consequent enhancement of the Λ_c production for $p_T < 3-4\,GeV$ at both RHIC and LHC energies. Furthermore, in fig.2 we present results for charmed hadron production in pp collisions at top LHC energy using a similar approach for AA collisions considering an hybrid hadronization via coalescence and fragmentation. The calculations for pp collisions were obtained assuming the formation of a QGP medium with a typical size estimated in hydrodynamics and transport calculations [34, 35]. For pp collisions shown in the right panel of fig. 1 we observe that the contribution of fragmentation is the dominant mechanism for the production of D^0 in all the p_T range explored where coalescence gives only a few percent of contribution. As shown in AA the coalescence contribution is significantly larger and comparable to the fragmentation one. Finally, as shown in the last panel the coalescence mechanism is the dominant mechanism for the Λ_c production. In general, the hybrid hadronization approach via coalescence and fragmentation predicts a rise and fall behaviour in the baryon-to-meson ratio in nucleus-nucleus collisions (AA). The left and middle panels of fig. 3 show the comparison between RHIC and LHC regarding the transverse momentum dependence of the Λ_c/D^0 ratio at mid-rapidity. As shown in fig. 3, the ratio decreases with increasing energy, moving from RHIC to LHC collisions. This trend can be attributed to the flattening of the charm quark spectrum from RHIC to LHC, indicating a higher numbers of mini-jets at LHC compared to RHIC, resulting in increased Λ_c production from fragmentation and consequently a smaller ratio than at RHIC. The final ratio represents a weighted average between the coalescence and fragmentation ratios [25]. Conversely, in pp collisions, the assumption of a formation of a small-medium in these collisions naturally accounts for the system size dependence

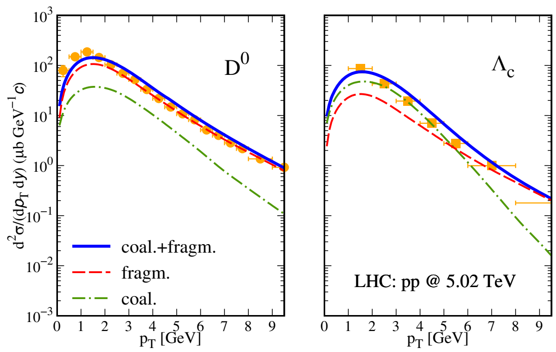

Fig. 2. – Transverse momentum spectra for D^0, and Λ_c baryon at mid-rapidity for pp collisions. Green dot-dashed and red dashed lines refer to the spectra from only coalescence and only fragmentation respectively, the blue solid line is the sum of fragmentation and coalescence. Experimental data taken from refs. [36-38].

of the charmed baryon-to-meson ratio, consistent with recent experimental data from pp collisions at LHC energies [36]. The right panel of fig. 3 shows this ratio for pp collisions at LHC mid-rapidity with $\sqrt{s} = 5.02, TeV$. It's worth noting that results obtained within the hybrid hadronization approach via coalescence and fragmentation gives similar results to the Statistical Hadronization Model (SHM) for D^0, D^*, and Λ_c, but showing significant differences for Ξ_c and Ω_c when compared to statistical models with an equal number of resonances [19, 27]. Finally, in the right panel of fig. 3 , we show the Ξ_c and Ω_c to D^0 ratios in pp collisions at $\sqrt{s} = 5.02\,TeV$. We compare the results obtained within coalescence and fragmentation with the experimental data from ALICE collaboration [18]. For both cases we obtain a ratio that is enhanced by the presence of the recombination process. The bands take into account for the uncertainty of the

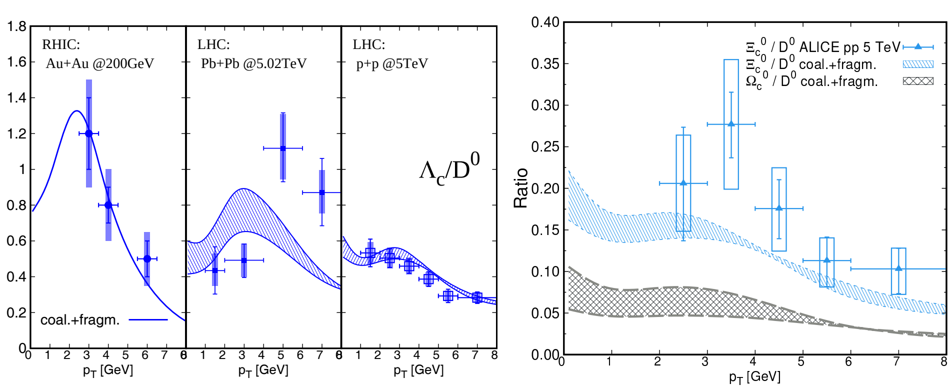

Fig. 3. – Left: Λ_c/D^0 ratio as a function of the transverse momentum at mid-rapidity for $Au+Au$ at $\sqrt{s} = 200\,GeV$ [39] (left panel), for $Pb + Pb$ at $\sqrt{s} = 5.02\,TeV$ [40] (middle panel) and $p + p$ at $\sqrt{s} = 5\,TeV$ [36] (right panel). The blue bands are the results obtained with coalescence plus fragmentation. Right: Ω_c/D^0 and Ξ_c/D^0 ratios as a function of the transverse momentum at mid-rapidity for $p + p$ at $\sqrt{s} = 5\,TeV$. Data taken from ref. [18].

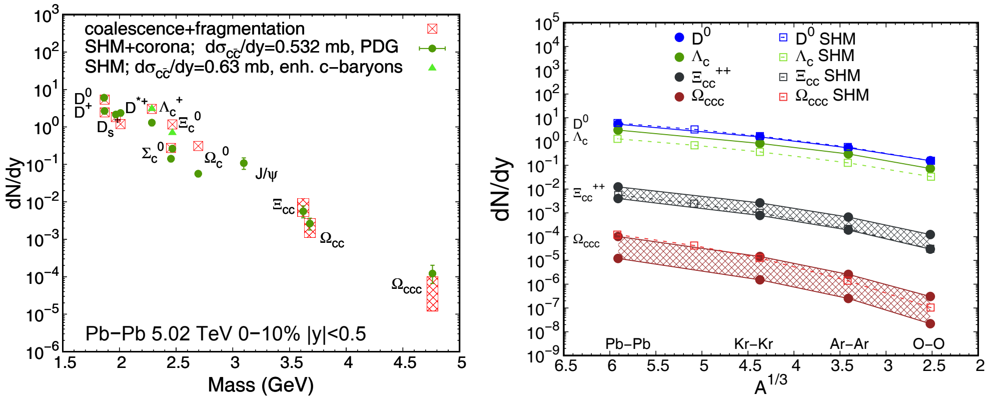

Fig. 4. – Left panel: Charmed hadron yields in PbPb collisions at mid-rapidity at 5.02TeV. Green symbols represent results obtained with SHM, while the red bands correspond to the results obtained by the hybrid hadronization through coalescence and fragmentation. The upper limit of the band corresponds to the yields obtained with realistic simulations, while the lower limit corresponds to the results obtained assuming a thermal distribution. Right panel: dN/dy at mid-rapidity of single and multi-charmed hadrons as a function of the size of the systems $A^{1/3}$. Open symbols represent SHM calculations, and filled symbols depict results obtained within coalescence plus fragmentation.

Wigner function widths, where we have considered variations of 20% for the particles radius involved in the ratio.

4. – Multi-charmed hadrons in different collision systems

In this section we focus on the yields of single charmed and multi-charmed baryons, particularly emphasizing Ξ_{cc} and Ω_{ccc} production, considering $Pb + Pb$ collisions and subsequently exploring system size dependence through smaller systems like $Kr + Kr$, $Ar + Ar$, and $O + O$ collisions. In the left panel of fig. 4, the yields for single and multi-charmed hadrons in $Pb+Pb$ collisions, covering $(0-10\%)$ centrality at mid-rapidity, have been shown within coalescence plus fragmentation approach. These results are compared with those from the Statistical Hadronization Model (SHM), in which an enhanced set of charmed baryons beyond those listed by the PDG are include, as in refs. [26-28]. In the figure, the lower limit in the band represents the yields obtained with realistic distributions, while the upper limit corresponds to the calculation considering thermal distributions for charm quarks. The hybrid hadronization approach with coalescence plus fragmentation exhibits a significant sensitivity to the underlying charm distribution function for multi-charmed baryons such as Ξ_{cc}, Ω_{cc}, and Ω_{ccc}. In particular, when a thermalized charm distribution is assumed, the model predicts an enhancement of the yields compared to those predicted by a realistic distribution, as indicated by the upper and lower limits in the band. This behavior arises from the presence of a larger number of charm quarks that can be found within a small momentum region for a thermal distribution. This has the effect to facilitate the coalescence mechanism compared to a more realistic distribution. Consequently, this property leads to an overall enhancement in the total yields and compared to single-charmed hadrons providing yields of Ξ_{cc}, Ω_{cc}, and Ω_{ccc} more sensitive to the charm distribution function. As discussed, multi-charmed hadrons are sensitive to the quark distribution function, making it interesting to study their production in various collision systems where the quark distribution may differ. We have examined the production of multi-charmed hadrons in different collision systems, including $Pb + Pb$, $Kr + Kr$, $Ar + Ar$, and $O + O$ collision systems. The initial p_T distribution used for these systems is based on pQCD calculations such as FONLL calculations. The initial charm distribution evolves within a QGP medium described by a relativistic Boltzmann approach; for details, refer to ref. [31]. As collision systems decrease in size from larger to smaller ones, the fireball's lifetime is reduced. Consequently, in smaller collision systems, the final transverse momentum distributions of charm quarks are flatter compared to those in $Pb + Pb$ collisions. In the right panel of fig. 4, the dN/dy obtained through the coalescence plus fragmentation approach for each species is shown as a function of the system size $A^{1/3}$. As shown in the left panel, the upper limit of the band corresponds to a fully thermalized charm distribution, while the lower limit represents the results obtained using the charm distribution derived from solving the Boltzmann transport approach. Open symbols in the right panel of fig. 4 represent dN/dy obtained by SHM. The comparison with SHM reveals that the yields exhibit a similar, albeit different, scaling with decreasing the size of the system $A^{1/3}$.

REFERENCES

[1] Dong X. and Greco V., *Prog. Part. Nucl. Phys.*, **104** (2019) 97.
[2] He M., van Hees H. and Rapp R., *Prog. Part. Nucl. Phys.*, **130** (2023) 104020.
[3] Andronic A. *et al.*, *Eur. Phys. J. C*, **76** (2016) 107.
[4] Gossiaux P. B. and Aichelin J., *Phys. Rev. C*, **78** (2008) 014904.
[5] He M., Fries R. J. and Rapp R., *Phys. Rev. Lett.*, **110** (2013) 112301.
[6] Uphoff J., Fochler O., Xu Z. and Greiner C., *Phys. Lett. B*, **717** (2012) 430.
[7] Cao S., Qin G.-Y. and Bass S. A., *Phys. Rev. C*, **92** (2015) 024907.
[8] Scardina F., Das S. K., Minissale V., Plumari S. and Greco V., *Phys. Rev. C*, **96** (2017) 044905.
[9] Das S. K., Ruggieri M., Scardina F., Plumari S. and Greco V., *J. Phys. G*, **44** (2017) 095102.
[10] Das S. K., Plumari S., Chatterjee S., Alam J., Scardina F. and Greco V., *Phys. Lett. B*, **768** (2017) 260.
[11] Das S. K., Scardina F., Plumari S. and Greco V., *Phys. Lett. B*, **747** (2015) 260.
[12] Plumari S., Coci G., Minissale V., Das S. K., Sun Y. and Greco V., *Phys. Lett. B*, **805** (2020) 135460.
[13] Oliva L., Plumari S. and Greco V., *JHEP*, **05** (2021) 034.
[14] Beraudo A., De Pace A., Monteno M., Nardi M. and Prino F., *JHEP*, **05** (2021) 279.
[15] Sambataro M. L., Sun Y., Minissale V., Plumari S. and Greco V., *Eur. Phys. J. C*, **82** (2022) 833.
[16] Sambataro M. L., Minissale V., Plumari S. and Greco V., *Phys. Lett. B*, **849** (2024) 138480.
[17] Lisovyi M., Verbytskyi A. and Zenaiev O., *Eur. Phys. J. C*, **76** (2016) 397.
[18] Acharya S. *et al.*, *JHEP*, **10** (2021) 159.
[19] Minissale V., Plumari S. and Greco V., *Phys. Lett. B*, **821** (2021) 136622.
[20] Beraudo A., De Pace A., Pablos D., Prino F., Monteno M. and Nardi M., arXiv:2306.02152 [hep-ph] (2023).
[21] Zhao J., Aichelin J., Gossiaux P. B. and Werner K., arXiv:2310.08684 [hep-ph] (2023).
[22] Greco V., Ko C. M. and Levai P., *Phys. Rev. Lett.*, **90** (2003) 202302.

[23] Minissale V., Scardina F. and Greco V., *Phys. Rev. C*, **92** (2015) 054904.
[24] Oh Y., Ko C. M., Lee S. H. and Yasui S., *Phys. Rev. C*, **79** (2009) 044905.
[25] Plumari S., Minissale V., Das S. K., Coci G. and Greco V., *Eur. Phys. J. C*, **78** (2018) 348.
[26] He M. and Rapp R., *Phys. Rev. Lett.*, **124** (2020) 042301.
[27] He M. and Rapp R., *Phys. Lett. B*, **795** (2019) 117.
[28] Andronic A., Braun-Munzinger P., Köhler M. K., Mazeliauskas A., Redlich K., Stachel J. and Vislavicius V., *JHEP*, **07** (2021) 035.
[29] Zhao J. *et al.*, arXiv:2311.10621 [hep-ph] (2023).
[30] He M. and Rapp R., *Phys. Rev. Lett.*, **131** (2023) 012301.
[31] Minissale V., Plumari S., Sun Y. and Greco V., arXiv:2305.03687 [hep-ph] (2023).
[32] Gossiaux P. B., Bierkandt R. and Aichelin J., *Phys. Rev.C*, **79** (2009) 044906.
[33] Peterson C., Schlatter D., Schmitt I. and Zerwas P. M., *Phys. Rev. D*, **27** (1983) 105.
[34] Weller R. D. and Romatschke P., *Phys. Lett. B*, **774** (2017) 351.
[35] Greif M., Greiner C., Schenke B., Schlichting S. and Xu Z., *Phys. Rev. D*, **96** (2017) 091504.
[36] Acharya S. *et al.*, *Phys. Rev. C*, **104** (2021) 054905.
[37] Acharya S. *et al.*, *Phys. Rev. Lett.*, **127** (2021) 202301.
[38] Acharya S. *et al.*, *Eur. Phys. J. C*, **79** (2019) 388.
[39] Adam J. *et al.*, *Phys. Rev. Lett.*, **124** (2020) 172301.
[40] Acharya S. *et al.*, *Phys. Lett. B*, **839** (2023) 137796.